


Article

A Minimal CA-Based Model Capturing Evolutionarily Relevant Features of Biological Development

Miguel Brun-Usan ^{1,*} , Javier de Juan García ² and Roberto Latorre ² ¹ CABD-Centro Andaluz de Biología del Desarrollo, CSIC-Universidad Pablo de Olavide, Campus UPO, 41013 Seville, Spain² Departamento Ingeniería Informática, Escuela Politécnica Superior, Universidad Autónoma de Madrid, 28049 Madrid, Spain; roberto.latorre@uam.es (R.L.)

* Correspondence: miguel.brun@csic.es

Abstract

Understanding how complex biological forms emerge and evolve remains a central question in evolutionary and developmental biology. To explore this complexity, we introduce a minimal two-dimensional, cellular automaton (CA)-based model that captures key features of biological development—such as spatial growth, self-organization, and differentiation—while remaining computationally tractable and evolvable. Unlike most abstract genotype–phenotype mapping models, our approach generates emergent morphological complexity through spatially explicit rule-based interactions governed by a simple genetic vector, resulting in self-organized patterns reminiscent of biological morphogenesis. Using simulations, we show that, as observed in empirical studies, the resulting phenotypic distribution is highly skewed: simple forms are common, while complex ones are rare. The model exhibits a strongly non-linear genotype-to-phenotype mapping in such a way that small genetic changes can lead to disproportionately large morphological shifts. Notably, transitions toward complexity are less frequent than regressions to simplicity, reflecting evolutionary asymmetries observed in natural systems. We further demonstrate that, by allowing for mutations in the generative rules, our model is capable of adaptive evolution and even reproducing generic features of tumoral growth. These findings suggest that even minimal developmental rules can give rise to rich, hierarchical patterns and complex evolutionary dynamics, positioning our CA-based model as a powerful tool for investigating how developmental constraints and biases shape morphological evolution.

Keywords: cell automaton; self-organization; genotype-phenotype-map; spatial pattern; complexity; evolvability

MSC: 37N25; 68Q80; 92C15



Academic Editor: Daniela Zaharie

Received: 5 September 2025

Revised: 24 September 2025

Accepted: 7 October 2025

Published: 9 October 2025

Citation: Brun-Usan, M.; de Juan García, J.; Latorre, R. A Minimal CA-Based Model Capturing Evolutionarily Relevant Features of Biological Development. *Mathematics* **2025**, *13*, 3238. <https://doi.org/10.3390/math13193238>

Copyright: © 2025 by the authors. Licensee MDPI, Basel, Switzerland. This article is an open access article distributed under the terms and conditions of the Creative Commons Attribution (CC BY) license (<https://creativecommons.org/licenses/by/4.0/>).

1. Introduction

Self-organization is a fundamental principle observed across all levels of biological organization, from molecular assemblies to ecological systems [1,2]. The spontaneous emergence of ordered patterns from local interactions has been extensively explored in developmental biology and evolutionary theory [3–5]. One of the clearest manifestations of self-organization in biology is the developmental process, whereby complex morphological structures emerge through the iterative and dynamic interplay between genes and cells [6].

During development, genes interact in structured gene regulatory networks (GRNs) controlling cellular properties and behaviors such as proliferation, polarity, apoptosis,

and migration [6–8]. The activation of these behaviors, embedded within the spatial context of tissues, collectively shapes the morphology of the developing embryo which, in turn, may potentially affect gene regulation via the channeled diffusion of morphogens or stress-driven mechanotransduction. This effectively creates a dynamic, recursive loop between gene activity and physical form.

This feedback-driven system ensures that successive developmental stages or spatial patterns (understood as specific distributions of cell types) differ from, and are often more complex than, preceding ones (which may be as simple as a spherical zygote), ultimately culminating in highly structured multicellular forms. Beyond this increase in morphological complexity, development introduces non-linearities into the relationship between genotype and phenotype. As a result, the *genotype-to-phenotype map* (hereafter GPM) of most organisms is inherently complex [9], a property that appears to extend to the relationship between the initial pattern or conditions and the final phenotypic outcomes—the so-called *epigenotype-to-phenotype map* [10]. Consequently, some phenotypes (especially simpler ones [11,12]) are more likely to arise than others, while some may be entirely inaccessible through developmental dynamics alone, leading to a morphospace with structured gaps and directional biases [13,14].

These intricacies arising from development are extremely relevant from an evolutionary point of view, as they can constrain phenotypic variation [15–17], reduce the efficiency of natural selection by introducing trait correlations [11], or channel evolution along non-adaptive trajectories [13,18–20]. However, despite their importance, characterizing the GPM in real organisms remains technically challenging, not only because it requires large-scale mutational screening, but also because many mutants result in non-viable forms. Leveraging data from natural populations is not always a viable alternative either, as most non-adaptive phenotypic variants, although developmentally accessible, are likely to have been purged over generations by purifying selection [21].

To address these limitations, many researchers have turned to computational models to study development and the structure of GPMs. Under the premise of biological realism, some of these models [22–26] simulate GRNs, morphogen diffusion, physics-based tissue biomechanics in a continuous 2D or 3D space, along with biologically inspired cellular behaviors, to recreate actual organs or phenotypes. These models typically rely on specific initial conditions, genetic programs, and developmental mechanisms, with minimal variation across replicates and/or generations [11,27,28]. Moreover, the number of potential interactions, and consequently, the computational demands, increase rapidly with the number of genes and cells [29]. Therefore, while very effective and informative for studying developmental dynamics of specific organs, these models are generally unsuitable for evolutionary studies involving large populations and high generational turnover.

At the other extreme are more abstract and highly idealized models which, although intended to capture certain properties of developmental dynamics, fail to implement self-organizing mechanisms [30]. These models typically compute the genotype-to-phenotype translation in a single step, relying on statistical correlations between genotypic and phenotypic changes (e.g., G-matrices encoding trait covariation [19,20,31]), or on mathematical functions that mimic developmental variation [32–34]. While computationally efficient (the phenotype is calculated in a single step from “genetic” parameters), these models lack many evolutionarily relevant features of real developmental systems, such as the physical space in which phenotypes emerge, emergent collective behaviors [3], gaps in morphospace [9,17,28], persistent developmental biases [16], or evolutionary novelties [35].

Situated between the physics-based models in continuous space and the non-generative models lacking explicit space lie the so-called cellular automata (CA): discrete, grid-based systems in which each cell updates its state according to fixed rules based on

its neighbors [36–38]. By operating in discrete space (often bidimensional) with limited discrete (often binary) cell states, CAs retain spatial structure, context-dependence, and rule-based emergent behavior while minimizing computational complexity, therefore offering a promising balance between generative capacity and computational simplicity.

One of the simplest and most well-known CA-models is the classical Conway’s Game of Life [39,40], a binary-state automaton implemented on a square grid (although several extensions—e.g., *HexLife* and *HighLife* [41,42]—have expanded its rule space and behavior). Despite its simplicity, this CA generates remarkably complex dynamics, including stable structures, periodic oscillators, and mobile patterns such as “gliders” and “spaceships”. Notably, a related one-dimensional automaton, *Rule 110*, has been proven Turing-complete (i.e., computationally universal), demonstrating the generative potential of CAs [43]. Another particularly interesting example is *Lenia* [44], a CA with continuous state values that exhibits life-like dynamics and emergent structures, albeit at a greater computational cost. However, despite their popularity in computer science, recreational mathematics, and theoretical physics, pure (i.e., deterministic) CA models are often unsuitable for biological processes due to their limited degrees of freedom and interpretability (however, see [29]).

In the cases where CAs have been applied to biological scenarios, they are usually designed to explore the evolution of ecological communities by establishing analogies between CA rules and biological processes [45]. For instance, in the Conway’s Game of Life, cells with too few or too many neighbors are said to “die” due to under- or overpopulation [40]. This population-level behavior can be extended to developmental patterning [46]. In a developmental context, the spatial patterns that emerge from neighborhood-based rules may be viewed as epigenetic, in the sense that they influence the final configuration of cell states (i.e., the phenotype) without modifying the generative rules of the system (i.e., the CA’s update rules, analogous to the genome) [47,48]. However, epigenetic mechanisms alone are insufficient to produce orchestrated developmental processes, as they also require genetic regulation to ensure robustness and heritability [10,49,50]. Furthermore, genetic mutations—i.e., changes in the generative rules of the genetic program—are essential for evolution as a source of heritable variation. These genetic dimensions of development and evolution have been incorporated into more biologically grounded CA-based models, such as the Cellular Potts Model (CPM) [27,51], which allows for a more fine-grained implementation of cell behaviors and biologically meaningful parameters [29].

In general, genetic control over cell states and behaviors is integrated into CPMs in the form of continuous or Boolean gene regulatory networks (GRNs), often combined with long-range cell–cell signaling and stochastic noise to prevent the system from becoming trapped in local energy minima [29,52]. In addition to cell signaling, CPMs typically rely on other non-local energy functions (such as constraints on surface/volume or perimeter/area ratios, adhesion energies, etc.) that are minimized across the entire system to maintain the physical integrity and viscoelastic properties of cells [29]. Another key feature of CPMs and related models is that each grid cell does not correspond to a single “biological” (in silico) cell, but rather to a fraction of subcellular volume, allowing for cell shape to vary dynamically in response to mechanical and tensile forces [27,29,53–55].

These additional layers of biological realism, together with the incorporation of CPM-based cores into multi-purpose modeling platforms like *CompuCell3D* [52], *MorphoSim* [56], *Morpheus* [57], and *Chaste* [29,58], have expanded the application domain of CAs to a broad variety of developmental systems. Examples include cell sorting [29,53,54], vertebrate limb bud morphogenesis [59], cell colony growth [55], organoid development [60], and somite segmentation [61], to name just a few.

However, in many of these models, cell signaling and morphogen diffusion, as well as gene–gene interactions (i.e., GRNs whose size scales with the square of the number

of genes), are typically formulated as systems of ordinary differential equations (ODEs) that require fine-grained numerical integration methods such as Euler–Maruyama [29]. Furthermore, many CPM-based models rely on asynchronous cell updates, which introduces additional stochasticity and computational overhead (although similar behaviors have been observed in synchronous update schemes [62]). Even in simplified CPM implementations designed to minimize algorithmic complexity, additional adjustments (not always formally supported [63]), such as allowing for multiple cells per grid site, are sometimes used to enhance biological realism [55,64]. Consequently, most CPM-based models exhibit relatively high computational complexity [56], with some approaching the cost of continuous-space simulations (e.g., *EmbryoMaker* [24–26]) and being similarly demanding in terms of computational resources [65].

This leaves a conceptual and methodological gap between simple, discrete, and deterministic cellular automata (e.g., Conway’s Game of Life) and complex CA-based developmental models designed to accurately describe real-world biological systems (e.g., the Cellular Potts Model). In this work, we introduce a minimal, biologically inspired CA-based model that helps fill this sparsely populated intermediate spectrum. Like other CAs, our model operates on a two-dimensional grid, updating cell states synchronously according to a few simple, local, and developmentally inspired rules [6,29,66]. In addition, our model implements a non-local rule, reminiscent of directional cell growth, that modifies neighboring rather than focal cells (a property that has been explored in some recent CA-based model variants [29,55]). As we show, this rule naturally gives rise to a form of volume-exclusion principle, even within the minimal architecture proposed here (see Section 4). This non-local growth, together with other biologically inspired minimal transformation rules, are encoded in a mutable vector that allows for evolutionarily adaptation (as in [50,67]).

Through extensive (>10,000) simulations and a variety of metrics, we demonstrate that our model exhibits key properties of biological development such as the generation of complexity via self-organized processes, multi-level hierarchy, skewed distribution of phenotypic complexity (more complex structures are less frequent), non-linear genotype-to-phenotype mapping, and evolvability. Furthermore, we offer a proof of principle for its heuristic potential by assessing (i) the interplay between genetic and epigenetic inheritance (i.e., maternal effects) under different selection criteria and (ii) its ability to quantitatively reproduce generic features of tumor growth. Given its algorithmic simplicity and computational efficiency, our model provides a minimal yet flexible tool for investigating the evolutionary consequences of complex developmental processes, with broad applicability to theoretical research in evolutionary and developmental biology.

2. Methods: The Model

The model (Figure 1) follows the typical structure of a two-dimensional cellular automaton with open boundary conditions (periodic or toroidal boundary conditions could potentially introduce artifacts if the boundaries were ever approached). Each row i and column j ($i \in \mathbb{Z}, j \in \mathbb{Z}$) in the lattice has associated a discrete variable S_{ij} , which is zero for empty positions and positive for positions containing living cells. For living cells, $S_{ij} \in \{1, \dots, 8\}$, encoding a spatial direction among the eight possibilities defined by Moore’s neighborhood. Therefore, at each iteration t , the whole system is defined by the set of internal states of all cells, that is,

$$\mathbf{S}^t = \{S_{ij}^t\}$$

Living cells can perform four different behaviors (or developmental rules) depending on the number of living neighbors in their Moore neighborhood:

- **Rule 0 (stasis):** The cell remains unchanged and alive in the next time step: $S_{ij}^t = S_{ij}^{t-1}$.
- **Rule 1 (apoptosis):** The cell dies: $S_{ij}^{t-1} = x \rightarrow S_{ij}^t = 0$. Besides the genetic regulation of cell death (see below), this rule is applied by default whenever a cell has zero living neighbors to ensure the physical continuity and integrity of the system.
- **Rule 2 (change of internal state):** The cell updates its state: $S_{ij}^t = S_{ij}^{t-1} + 1$; if $S_{ij}^{t-1} = 8$, then $S_{ij}^t = 1$. Note that while other increments in Rule 2 (e.g., +2, +3) are certainly possible, they would unnecessarily complicate the minimal nature of the model and diverge from biological systems, where non-gradual changes in cell states are typically achieved through gene regulatory network dynamics.
- **Rule 3 (growth):** The cell initiates the creation of a clone in the direction specified by its internal state S_{ij} , provided that the target cell is vacant. If the target location is already occupied by another living cell, no action is taken. Without loss of generality, directions are defined relative to the Moore neighborhood and indexed clockwise, starting from the cell directly above. Each direction is labeled using a two-letter code that combines vertical (U: Up; C: Central; D: Down) and horizontal (L: Left; C: Central; R: Right) references. Accordingly, $S_{ij} = 1$ corresponds to UC, $S_{ij} = 2$ to UR, $S_{ij} = 3$ to CR, $S_{ij} = 4$ to DR, $S_{ij} = 5$ to DC, $S_{ij} = 6$ to DL, $S_{ij} = 7$ to CL, and $S_{ij} = 8$ to UL.

Although these behaviors represent only a subset of the cellular mechanisms known in plants and animals [6–8,68], they underlie many important morphogenetic transformations and can be implemented even in a minimal architecture. In contrast, simulating more complex behaviors, such as cell shape changes that drive tissue deformation or migration, typically requires allowing for multiple grid sites per cell or multiple cells per grid unit [27,55,69], introducing continuous force fields coupled to the grid (as in lattice-gas or lattice-Boltzmann approaches [64,65,70]), or adding parameters to capture heterotypic adhesion strengths or chemical gradients, all of which significantly compromise the model's minimalism.

To avoid the complications outlined above and to make our four minimal key behaviors operative, they are encoded in a genetic vector \mathbf{G} of length 8, which is fixed at the beginning of the simulation and identical for every cell. Notice that, since the system's evolution cannot be formalized using local transition matrices (because a dividing cell S_{ij} may modify a different cell S_{kl} with $(k \neq i) \vee (l \neq j)$), the choice of a vector as the repository for the transformation rules provides a practical encoding of the cellular automaton (CA) rules. Such a direct encoding of the rules (rather than using a genetic network *per se*, whose size scales quadratically with the number of genetic elements) keeps the model minimal and compact while retaining a clear biological analogue to a linear genome, widely used in biological modeling [27,50,67,71]. Furthermore, this representation enables the digital “organisms” to undergo mutation or to perform genetic crossing [72,73] to explore the effects of genetic admixture (not addressed in this work, but see [50]).

At each time step, the number of living neighbors (N_{ij}) determines the update rule to be applied, and, therefore, the behavior of the corresponding cell. Specifically, the k -th value of the vector \mathbf{G} determines the rule to be applied to any cell with exactly k neighbors. More formally,

$$\text{IFF } (S_{ij} \neq 0 \wedge N_{ij} = k \wedge k \neq 0) \implies \text{cell } S_{ij} \text{ performs behavior } G_k,$$

$$\text{where } k \in \{1, \dots, 8\} \text{ and } G_k \in \{0, 1, 2, 3\}$$

In turn, since only living cells can perform “actions”, an initial population of such cells is required to begin the simulation. These cells constitute the initial conditions and can adopt different spatial configurations, encoded as a binary pattern in the matrix \mathbf{Epi} . This \mathbf{Epi} matrix, which defines the system's state at $t = 0$ (\mathbf{S}^0), may be interpreted as maternally

inherited epigenetic information, analogous to the zygotic mRNA gradients necessary to establish body axes in many organisms [74].

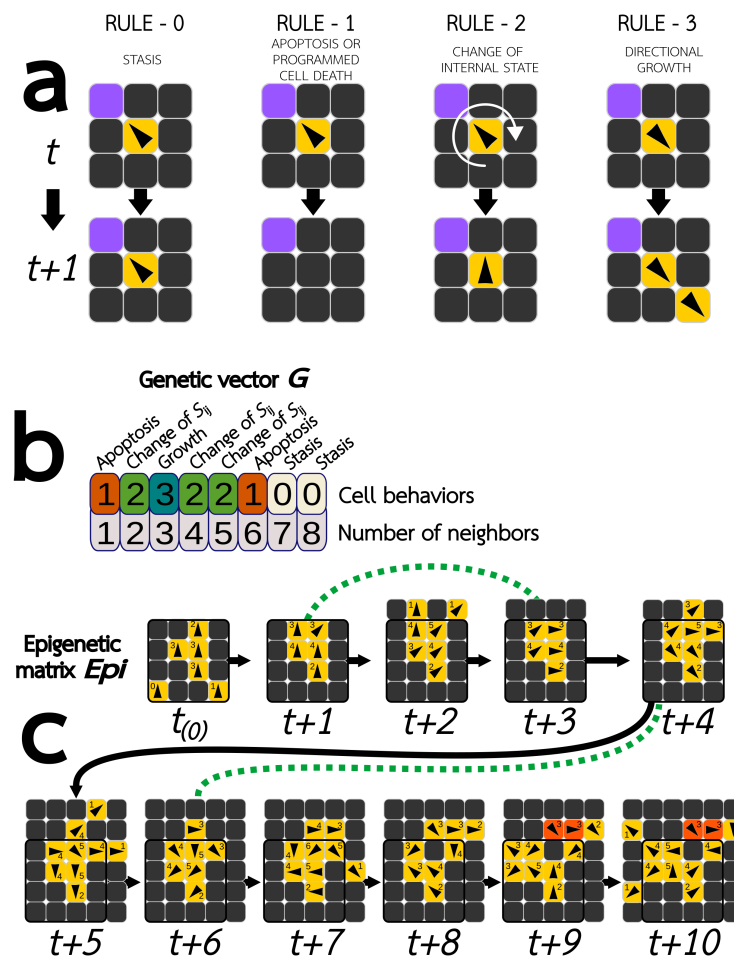


Figure 1. Graphical depiction of the proposed CA-based model. (a) Developmental rules—conceptualized as biologically inspired cell behaviors—implemented within our model, namely, Rule 0 (developmental stasis), Rule 1 (apoptosis or programmed cell death), Rule 2 (change of internal state in a clockwise fashion), and Rule 3 (directional cell growth). The yellow cell indicates the focal cell executing the behavior, with the central arrowhead representing its internal state (S_{ij}), which determines the direction of cell division (see Section 2). Purple and black cells represent living and dead neighboring cells, respectively. (b) An example genetic vector G encoding the possible rules to be executed by the focal cell. Each entry in G (from 1 to 8, bottom row) corresponds to the rule (top row) triggered when the focal cell has exactly that number of living neighbors. In this example, G specifies that apoptosis occurs with one or six neighbors; internal state changes occur with two, four, or five neighbors; and growth is triggered with three neighbors. (c) Illustrative dynamics over ten iterations using the genetic vector G from panel (b) and the “epigenetic” matrix Epi shown at $t_{(0)}$, which encodes the initial distribution of living cells in a 4×4 grid. For each living cell, small numbers indicate the number of living neighbors, and arrowheads represent the internal state. Orange cells denote those experiencing *frustration* (i.e., cases in which the developmental rule to be executed cannot proceed due to spatial constraints; see Discussion). This example illustrates the progressive, yet non-monotonic, increase in complexity observed in many parameter combinations, and how identical spatial patterns with different internal states (linked by green dotted lines) can lead to distinct morphogenetic transformations.

To ensure comparable magnitudes between the genetic and epigenetic spaces, the size of the initial prepattern Epi is set to $4 \times 4 = 16$ cells, each initialized with $S_{ij} = 1$. Thus, the epigenetic search space has $2^{16} = 65,536$ possible configurations, since each of the

16 positions in **Epi** can contain either a living cell or empty space. Similarly, the size of the genetic search space is $4^8 = 65,536$, where 4 is the number of possible rules (including Rule 0) and 8 is the length of the vector **G**. Combined, these yield a total evolutionary search space of $2^{16} \times 4^8 = 4,294,967,296$ possible configurations, which is large enough ($>10^9$) for the questions addressed in this work, yet easily expandable (see Section 4).

Given that the application of the aforementioned rules is fully deterministic (i.e., no probabilistic mechanisms are involved), the dynamic transitions of the system from state \mathbf{S}^t to the subsequent state \mathbf{S}^{t+1} depend solely on the current configuration and the behaviors encoded in the rule vector **G**. These state transitions across iterations can be denoted by the map \mathcal{R} :

$$\mathcal{R}(\mathbf{S}^t, \mathbf{G}) \rightarrow \mathbf{S}^{t+1}$$

For the sake of clarity, specific analytical techniques and experimental setups are described in the corresponding Results sub-sections.

3. Results

3.1. Complexity and Stability Analysis

We first explored the behavior of the system across a large number ($n = 10,000$) of parameter combinations (i.e., random pairings of random genomes **G** and random initial conditions **Epi**). Although this represents only 0.00025% of the total search space, previous research adopting similar approaches has shown that such sparse yet unbiased explorations are sufficient to uncover relevant variational properties of generative systems [11,49,75]. For each parameter combination, we ran the model for $t_{\max} = 150$ iterations (via a synchronous parallel update algorithm), recording the final spatial distribution of living cells as the resulting phenotype. Although these phenotypes do not resemble known biological organisms, a visual inspection reveals substantial variation in form and complexity, with patterns ranging from minute to large morphologies (Figure 2). Many phenotypes exhibit X- or Y-shaped structures that appear to function as *bauplans* for these digital organisms, i.e., basic templates from which further variation emerges. These often incorporate triangles, fractal-like motifs, and secondary patterns. The most complex phenotypes display a baroque mixture of structural elements at various scales, some even evoking the stylized hummingbirds of the Nazca petroglyphs. From a dynamical perspective, it is noteworthy that conserved structures (such as the radial “arms” defining the overall *bauplan*) emerge early during in silico developmental time (Figure 2m). In contrast, the finer patterning that introduces differentiation and amplifies the phenotypic impact of parameter variation tends to appear later, suggesting a temporal hierarchy in morphogenesis. This developmental sequence broadly parallels patterns observed in real-world embryogenesis, where coarse body plans precede detailed and species-specific structural elaboration [74,76].

As in real-world developmental systems, not every parameter combination gave rise to a viable phenotype. As shown in Figure 3a, four distinct dynamical regimes emerged in our simulations: extinction within a few iterations ($\approx 95\%$), steady-state or cyclic behavior ($\approx 3\%$), indefinite growth ($\approx 2\%$), and chaotic ($<1\%$). These proportions closely match those reported in theoretical models of real GRNs [28,77]. Notably, even among the phenotypes exhibiting indefinite growth, 99% remain bounded within the theoretical upper limit predicted by a two-dimensional random walk model (scaling as $n x / \log(x)$ with $n < 6$), and all simulations lie well below the x^2 curve, which would correspond to the unrestricted growth of a solid square.

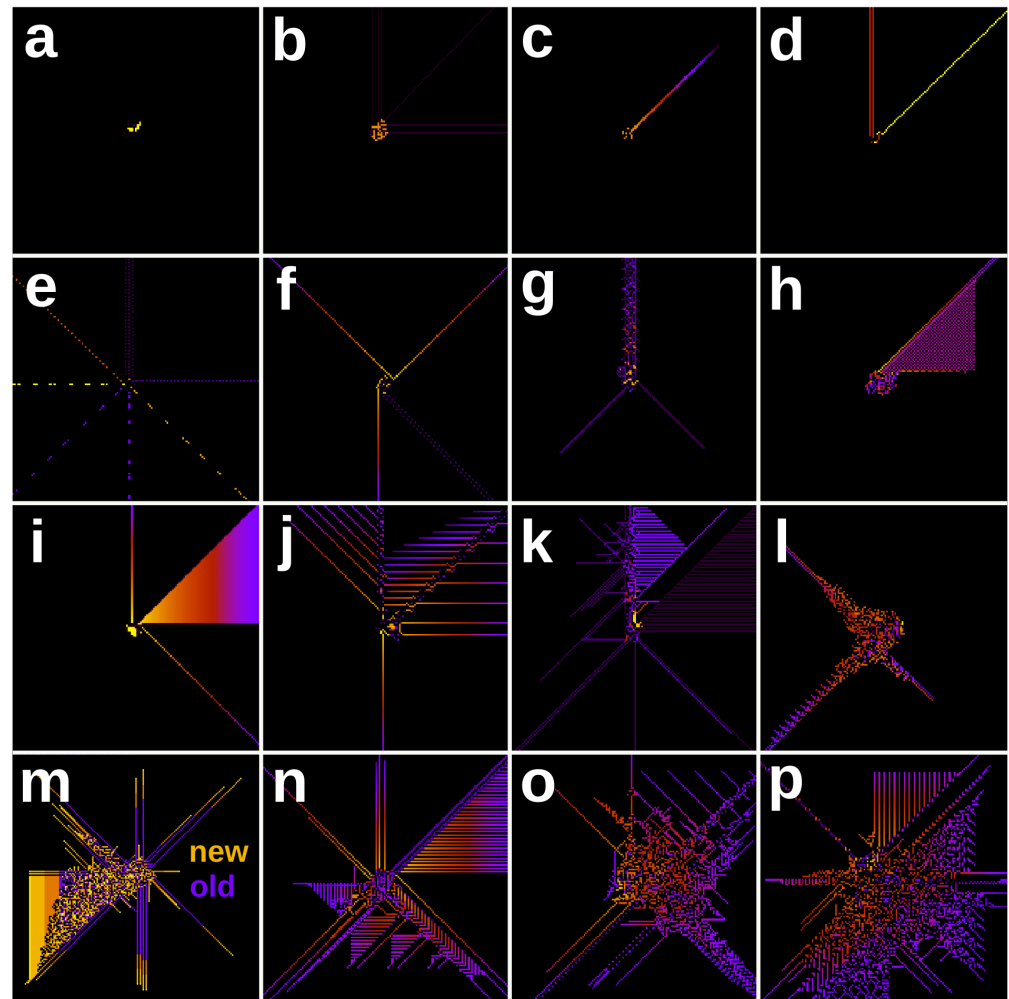


Figure 2. Bestiary of illustrative morphologies from our parametric exploration, sorted by increasing complexity. (a–f) Examples of low-complexity phenotypes, characterized by a small number of living cells forming simple patterns, low algorithmic and informational complexity, and near-linear parameter-to-phenotype mappings. (g–l) Mid-to-high-complexity phenotypes. Complexification often emerges from an X- or Y-shaped skeleton with additional finely patterned, secondary structures. (m–p) Representatives of the most complex phenotypes, characterized by large populations of living cells, intricate and surreal patterns reminiscent of the Nazca lines, high algorithmic/informational complexity, and non-linear mappings between parameters and phenotypes. In (m), colors represent cell age: purple cells (forming the “bauplan” skeleton) are developmentally old, having appeared during the first half of developmental time, whereas orange and yellow cells emerge later. In all other plots, colors encode a combination of each cell’s age and its internal state S_{ij} , using an arbitrary color code. Black regions indicate areas without living cells.

Phenotypic complexity was quantitatively assessed using three complementary measures: (1) size, defined as the final number of living cells (N_c); (2) Shannon entropy (H); and (3) algorithmic (Kolmogorov) complexity. Since the latter is formally incomputable [78], we followed standard practice and approximated it via lossless compression. Specifically, we used the compression ratio of phenotype data files, obtained with the standard *zipfile* module of *Python* 3.10, as a proxy. This method assumes that highly structured data can be efficiently compressed, whereas incompressible data lacking exploitable patterns require a description as complex as the data itself. All three complexity metrics yielded negatively skewed (approximately exponential) distributions, indicating that the more complex

the phenotype, the rarer its occurrence (Figure 3b). This pattern aligns with previous observations of organismal complexity [79].

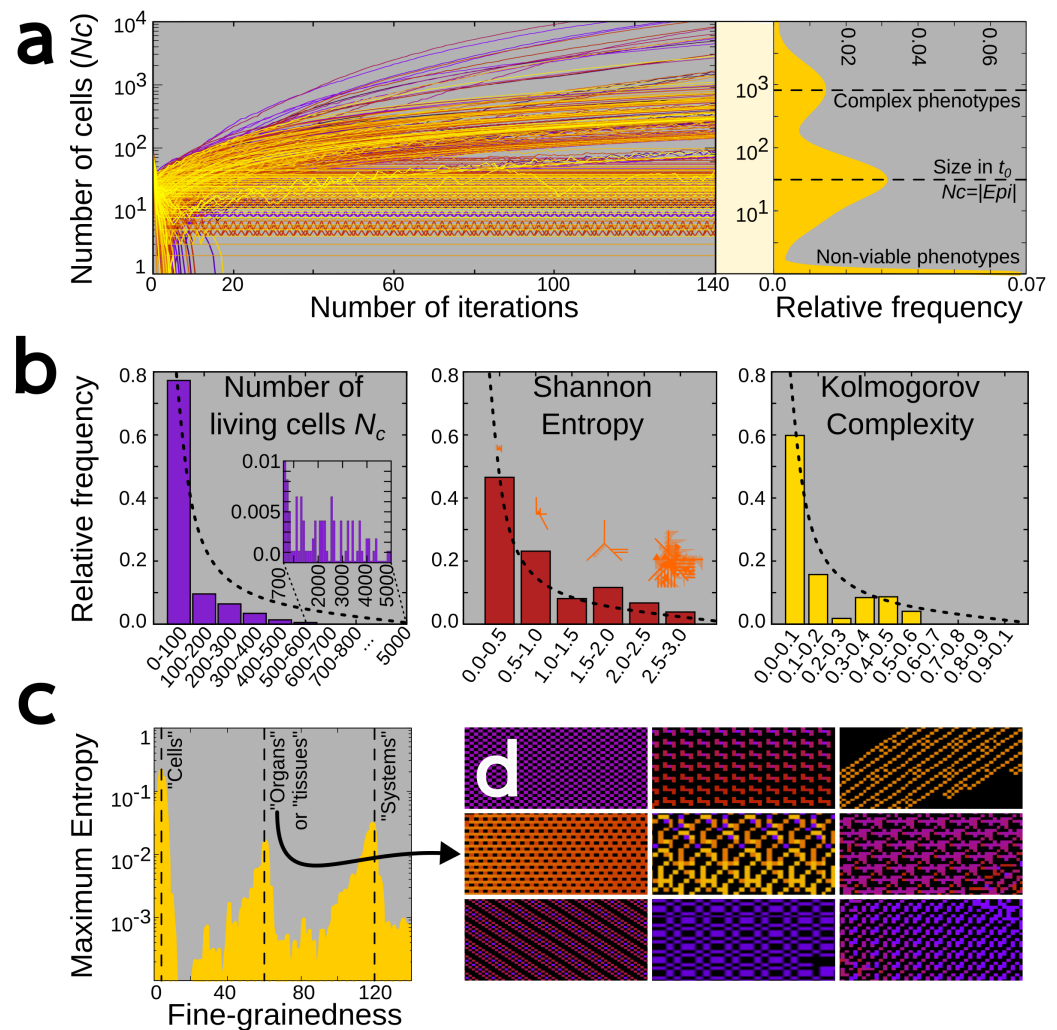


Figure 3. Complexity and stability analysis. (a) Developmental trajectories based on the number of living cells across 10,000 simulations with random initial conditions (**Epi**) and genetic vectors (**G**), revealing three distinct dynamical regimes: extinction, steady-state/cyclic behavior, and unbounded growth, with their respective frequencies. (b) Distributions of final phenotype complexity measured by number of living cells (N_c), Shannon entropy (H), and compression-based algorithmic complexity. All metrics show a non-linear decay with increasing complexity (dashed lines: exponential fit). Insets in the middle panel show representative phenotypes for selected complexity values. (c) Jensen–Shannon divergence across phenotypic scales reveals peaks in pattern redundancy at three characteristic sizes, suggesting emergent structural levels (see main text). (d) Zoom-ins of medium-scale motifs (at the “organ/tissue level”) that appear consistently with minimal variation within and across phenotypes (in arbitrary colorcode).

Importantly, pairwise comparisons revealed that the three complexity measures were only weakly correlated with one another (N_c vs. H : Pearson correlation coefficient $R = 0.234$; N_c vs. Kolmogorov: $R = 0.561$; Kolmogorov vs. H : $R = 0.232$). This lack of strong correlation indicates that each measure captures a distinct aspect of phenotypic organization, and that the negative relationship between complexity and frequency is a robust and metric-independent feature of the system. Furthermore, the final phenotype size (N_c) was also not correlated with the number of initially living cells in **Epi** ($R = 0.049$), suggesting that, as in other CAs and biological systems [9,80], initial conditions are poor predictors of the system’s behavior and long-term dynamics (see next section). Introducing

discrete random cell states $U \sim \{1, \dots, 8\}$ in **Epi** neither introduces a meaningful difference in the shape of complexity distributions (p -value $\approx 2.6 \times 10^{-6}$ for pairwise comparisons among N_c distributions using Wilcoxon signed-rank test). By contrast, increasing **Epi** size does affect the distributions, as it alters the λ parameters of the exponential fits, approximately following $\lambda \propto 1/\mathbf{Epi}$. These possibilities are only explored here in a limited way, since the parsimonious principle guiding our experiments favors keeping the model and its parametric space minimal.

To further investigate how phenotypic complexity is distributed across organizational levels, from individual “cells” to entire “organisms”, we conducted an information-theoretic analysis using the Jensen–Shannon divergence [81]. By applying a sliding window of variable size, we quantified the redundancy (or information content) of progressively smaller subsets of each phenotype. As shown in Figure 3c, complexity is not uniformly distributed across scales. Instead, the analysis reveals three main peaks in pattern redundancy at granularities roughly corresponding to subsets of $\sqrt{4} = 2$, $\sqrt{60} \approx 8$, and $\sqrt{120} \approx 11$ cells. These represent characteristic organizational levels at which local patterns appear especially ordered and exhibit high statistical regularity, suggesting that phenotypic complexity in our model is hierarchically organized. The smallest scale likely reflects basic empty space–living cell permutations between adjacent grid positions, whereas the largest scale appears to correspond to macroscopic features located along the main quadrants and axes, such as the “arms” of X- or Y-shaped forms. The intermediate peak may correspond to the scale at which self-organization is most effective, producing non-trivial structured motifs with internal coherence. Those medium-scale motifs (illustrated in Figure 3d) are of particular interest, as they constitute highly conserved substructures, analogous to tissues or serial organs, that emerge with minimal variation across different regions of a single phenotype and even among phenotypes generated by distinct genetic and epigenetic configurations.

The hierarchical organization of phenotypic complexity was further studied by analyzing the Hausdorff dimension (or “fractality”, HD) of the resulting phenotypes. Using the box-counting method [82], we estimated the Hausdorff dimension for the subset of simulations where this calculation was feasible (typically those with $N_c > 100$). The resulting distribution of dimensionalities followed a log-normal pattern, peaking around $HD \approx 0.65$. This value is strikingly close to that reported for classical Cantor dust-like structures ($HD \approx 0.63$) [83], suggesting that our CA-based model not only produces phenotypes of considerable complexity, but does so by generating nested substructures that hierarchically emerge from the inside out, exhibiting scale-invariant, fractal-like properties. In other words, the observed complexity is not merely a consequence of structural elaboration, but reflects an underlying generative logic capable of producing hierarchically organized, self-similar patterns.

3.2. Genotype-to-Phenotype Mappings

We next asked whether, as in real-world developmental systems, our CA-based model and its pseudo-developmental process exhibit a non-linear mapping between generative parameters (i.e., the genetic vector **G** and the **Epi** matrix) and resulting phenotypes. To address this, we analyzed how phenotypic divergence varies with genetic distance.

Genetic distance was quantified using the Hamming distance between the genetic vectors of individuals A and B (GHD), scoring each entry in the summation as 0 if $G_k^A = G_k^B$ and 1 otherwise. This binary definition avoids spurious distance inflation due to the arbitrary numerical coding of behavioral rules. Phenotypic distance was quantified by means of both Hamming distance (PHD) and a Euclidean distance (PED). PHD accounts only the living cell/empty space status in the resulting phenotypes (i.e., $S_{ij} \neq 0$ vs. $S_{ij} = 0$), while PED compares the full internal state values of all living cells S_{ij} .

As a first step, we sampled random pairs of individuals from the initial ensemble and compared their genetic and phenotypic distances. As shown in Figure 4a,b, GHD exhibits a saturating relationship with both PED and PHD, indicating that increasing genetic divergence does not necessarily lead to proportional phenotypic divergence. These results support that the GPM in our model is pervasively non-linear, affecting both the structural and functional aspects of phenotypes.

The same experimental procedure was repeated to assess the relationship between (Hamming) differences in initial conditions (Epi matrices) and the resulting phenotypes across pairs of individuals. Both PHD and PED were used to quantify phenotypic (dis-)similarity. The results (Figure 4c,d) indicate that, as in other biological systems (both real and simulated [10,84]), many general features of the epigenetic-to-phenotype map—including its degree of nonlinearity—are comparable to those observed in GPMs (cf. Figure 4, panels a,b vs. e,f).

A potential explanation for the observed saturating pattern, unrelated to the non-linearity of the GPM, is that it may be a statistical artifact resulting from saturation effects. Specifically, it is possible that, beyond a certain GHD threshold, phenotypic differences converge to the expected dissimilarity between two random binary matrices of size N . This effect would be especially pronounced around $\text{GHD} \approx 6$, which, according to the Central Limit Theorem, is the most probable Hamming distance between two random genetic vectors of length 8, where $\mathbb{P}(G_k^A \neq G_k^B) = \frac{3}{4} \cdot |G|$. In that case, the apparent non-linearity could simply reflect the intrinsic saturating growth pattern already observed in Figure 3a.

To rule out this possibility, we repeated the experiment while restricting GHD to the immediate mutational neighborhood. Specifically, we selected a random subset of genomes from the initial ensemble and, for each one, generated 30 mutants by introducing 1, 2, or 3 point mutations, each implemented as

$$G_k \rightarrow (G_k + 1) \bmod 4, \quad \text{with } k \sim \mathcal{U}\{1, |G|\}$$

Phenotypic distances were then computed between each mutant and its corresponding “wild-type” genome (Figure 4e), and also between mutant pairs within the same local neighborhood via pseudo-bootstrap sampling (Figure 4f). In both cases, the results show a saturating pattern, reinforcing the conclusion that the GPM is intrinsically non-linear across mutational scales. This similarity in the degree of non-linearity across scales suggests that the GPM may exhibit a self-similar, scale-free structure, a hallmark of many self-organizing dynamical systems [1] (see Section 4 for a probabilistic interpretation of this result).

To conclude our analysis, we explored how GPM behavior varies across the phenotypic complexity spectrum. Specifically, we restricted the analysis to the most complex ($H > 2.5$) and simplest ($H < 0.5$) phenotypic subsets from the initial ensemble, finding that simple phenotypes tend to be associated with more linear mapping, while complex phenotypes exhibit more intricate and discontinuous relationships (Figure 4g,h). This pattern is consistent with previous findings in biological models [11,25]. Furthermore, large-effect mutations not only produce greater morphological change, but also lead to more discrete and non-gradual transitions in phenotype space.

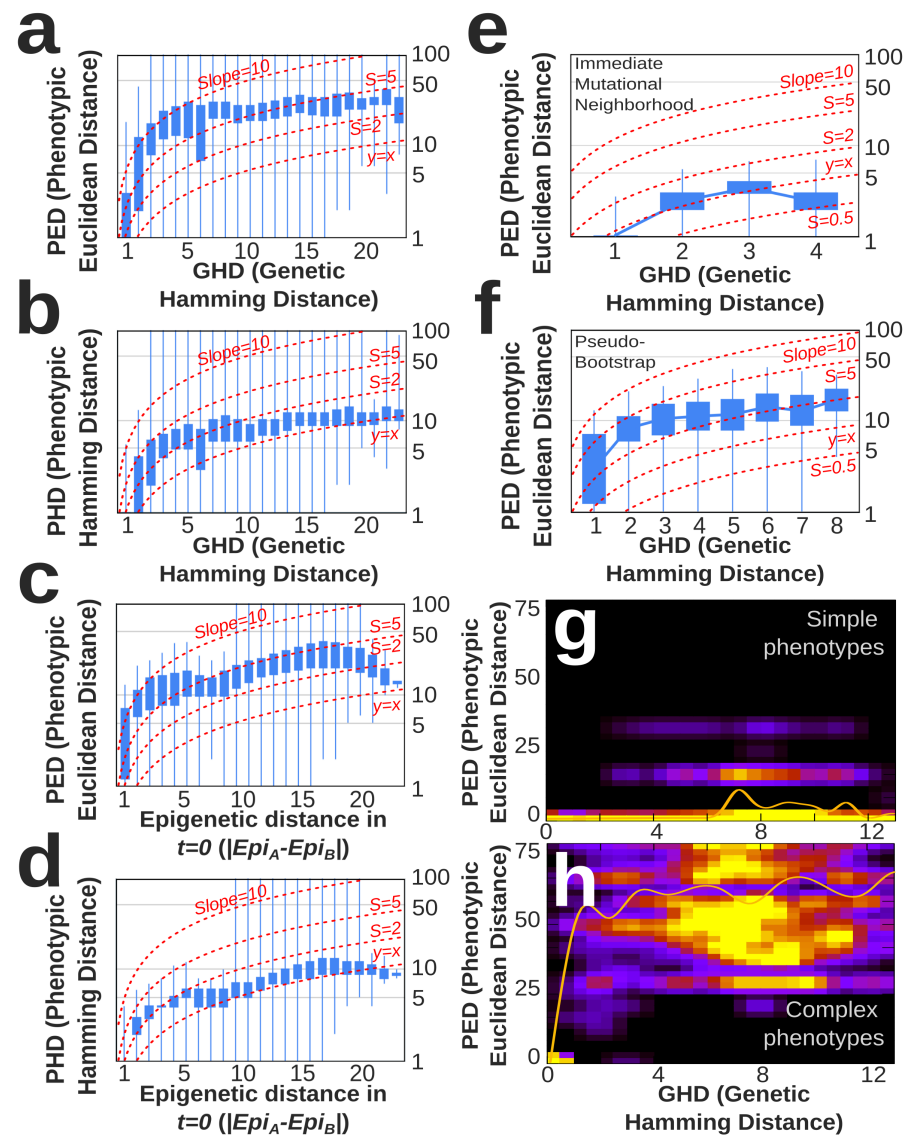


Figure 4. Relationship between genetic and phenotypic divergence. (a) PED vs. GHD for a subset of randomly chosen pairs of individuals from the initial ensemble. (b) PHD vs. GHD for the same pairs. Both panels reveal a non-linear, saturating pattern in the GPM, evidenced by their deviation from reference linear slopes (red dashed lines). (c,d) Analogous analyses as in (a,b), but relating Hamming differences in initial conditions (Epi matrices) to phenotypic differences. The results show a comparable degree of non-linearity in the epigenetic-to-phenotype map. (e) PED vs. GHD between each focal genotype from a randomly selected subset and its immediate mutational neighborhood (30 one-, two-, or three-step mutants). (f) PED vs. GHD between pairs of mutants within the same local mutational neighborhood (via pseudo-bootstrap). Panels e and f use PED, but qualitatively equivalent patterns were observed with PHD. The persistence of saturation confirms the non-linearity of the GPM at small genetic distances. (g,h) GPMs restricted to the most complex ($H > 2.5$) and simplest ($H < 0.5$) phenotypic subsets. In these heatmaps, yellow hues indicate high frequencies or occurrences, while purple tones correspond to low frequencies. Black regions represent zero frequency. Orange lines show smoothed average values. Overall, these heatmaps show that complex phenotypes exhibit more non-linear and discontinuous mappings, whereas simpler phenotypes tend to follow predominantly linear relationships.

3.3. Evolvability Assays

One of the core properties of our CA-based model—featuring mutable rules and initial conditions—is its capacity for adaptive evolution, a feature generally absent in CA

with fixed update rules. To assess this *evolvability*, we performed a series of experiments designed to test adaptive performance under different evolutionary scenarios.

In a first set of simulations, we implemented a standard mutation-selection-drift scenario [85], where a population of $p = 32$ individuals, randomly selected from the initial ensemble, evolved toward an arbitrary (fixed) target phenotype T , also drawn from the same initial ensemble. Evolution proceeded over discrete, non-overlapping generations, with 20% of individuals undergoing a single point mutation at each generation, unless otherwise stated (see below). The absolute fitness W of each individual A was defined as the inverse of its PHD to the target phenotype T :

$$W(A) = [1 + \text{PHD}(A, T)]^{-1}. \quad (1)$$

Relative fitness W^* ($0 < W^* < 1$), obtained by normalizing W to the maximum fitness in the population, determined the probability that each individual was selected to survive into the next generation under non-deterministic selection. Adaptation, in this context, was simply defined as a consistent increase in the average absolute fitness over time.

Since our model allows for variation in both genetic and epigenetic components, we performed three independent sets of simulations in which mutations affected (1) only the genetic vector **G**, (2) only the initial conditions **Epi**, or (3) both **G + Epi**. For each condition, 30 independent trials were performed to ensure statistical robustness.

Figure 5a–c illustrate the consistent increase in average absolute fitness W across the three mutational scenarios. Each panel compares the population average (red) with the best fitness reached up to each generation (all-time-high, ATH; blue), which also exhibits an asymptotic convergence toward $W = 1$. These general trends demonstrate the adaptive capacity of our CA-based model. Notably, panel d confirms that the initial generations in the simulations already capture the overall adaptive trend—even though, as expected, the magnitude of improvement ($\sim 20\%$) is modest under this evolutionary time constraint. These short-term fitness trends serve as a reliable proof-of-principle for evolvability, while also enabling robust comparisons between experimental conditions within a balanced trade-off between evolutionary resolution and computational cost.

To further evaluate the conditions under which adaptive performance is enhanced, we conducted a second set of simulations focused on the role of mutational distance between target and initial phenotypes. Specifically, we tested whether evolvability improves when the target phenotype lies within a closer (and presumably more accessible) region of the genotype space. In these simulations, a reference individual, randomly drawn from the initial ensemble, was selected to serve as the target phenotype T . Initial populations were then constructed from mutant variants generated at two predefined genetic distances, using the reference individual's genome as a template: *small* (two mutations) and *large* (six mutations, sufficient to induce substantial phenotypic divergence; see Figure 2a). As in the previous experiments, three mutation regimes were tested: modifying only **G**, only **Epi**, or both (**G + Epi**).

As shown in panels e and f of Figure 5 (cf. panel a), evolvability improves substantially when the target phenotype lies within a relatively close mutational neighborhood—even when that neighborhood still represents a considerable search space ($4^6 = 4096$ possible genotypes). This result reinforces the model's ability to navigate fitness landscapes effectively when evolutionary constraints are moderated. Furthermore, it aligns with well-established principles of evolutionary dynamics, which predict enhanced evolvability when the ratio between search space size and available evolutionary time is minimized. According to classical population genetics theory, adaptation could be further enhanced by increasing population size or fine-tuning mutation rates [72,73]. However, since the effects

of these parameters are well understood in the context of evolutionary dynamics, they were held constant in our simulations to isolate the specific contribution of mutational distance.

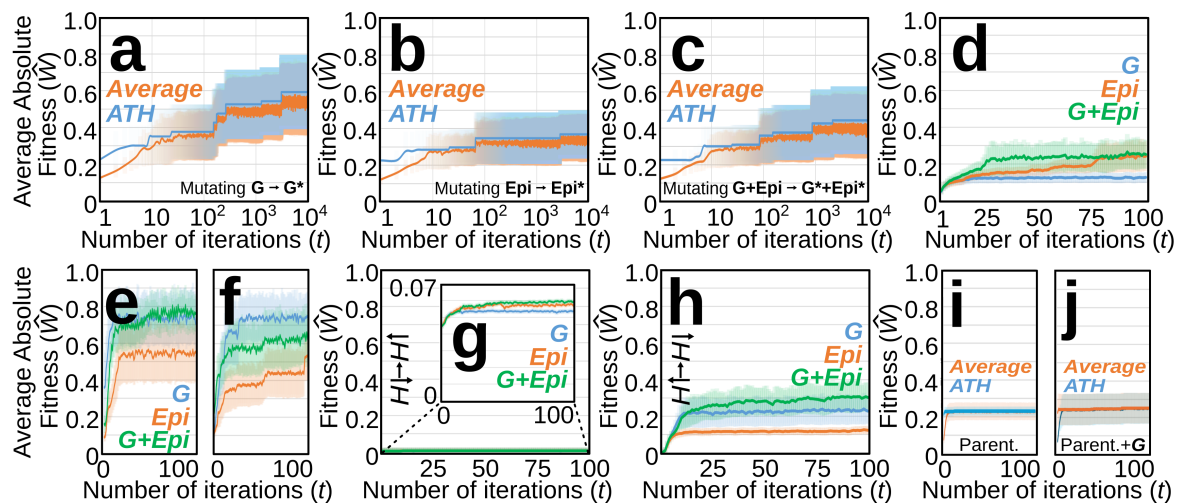


Figure 5. Evolvability assays. (a–c) Long-term evolutionary trajectories in simulations where mutations affect only the genetic vector **G** (a), only the epigenetic initial conditions **Epi** (b), or both (c). Orange lines show the evolution of average absolute fitness, and blue lines indicate the historical maximum or all-time-high (ATH) fitness at each generation. All scenarios exhibit a consistent upward trend, demonstrating adaptive potential. (d) Short-term trajectories of average fitness under the same mutation regimes: **G** (blue), **Epi** (orange), and **G + Epi** (green). While most populations eventually reach the target phenotype given sufficient evolutionary time ($W_{t \rightarrow \infty} = 1$), short simulations already capture the overall adaptive trend. (e,f) Short-term fitness trajectories when the target phenotype lies within a relatively small mutational neighborhood: $GHD \leq 2$ in (e) and $GHD \leq 6$ in (f). Evolvability improves in both cases, with the system exhibiting consistent gains across all mutation regimes, although adaptation slows as the mutational radius increases. (g,h) Short-term fitness trajectories for transitions between phenotypes of differing complexity. In (g), populations initialized with simple phenotypes ($H < 0.5$) evolve toward complex targets ($H > 2.5$), while in (h), the reverse occurs. Evolutionary transitions are asymmetric: simplification is rapid and reliable, whereas complexification is slower and often leads to fitness plateaus. (i,j) Short-term fitness trajectories under maternal effects with no buffering. In these simulations, each organism inherits its initial conditions from its maternal phenotype (see main text). Both with- and without-genetic-mutation setups (i vs. j) consistently fail to adapt, highlighting that unbuffered maternal inheritance undermines evolvability. All panels: population size $p = 32$, 30 replicates, non-deterministic selection.

Next, we explored whether the direction of evolutionary change shows an inherent bias related to the complexity of the target phenotype. In other words, we investigated whether transitions between phenotypes of different complexity occur with equal ease, or whether the system tends to favor either simplification or complexification. This type of asymmetry has been reported in various biological systems and may reflect a fundamental feature of developmentally mediated genotype–phenotype maps [12,86,87]. To test whether a similar bias arises in our model, we ran simulations on two independent populations of 32 individuals each: one initialized with low-complexity phenotypes ($H < 0.5$) and the other with high-complexity phenotypes ($H > 2.5$). Each population evolved toward a target of opposite complexity: from simple to complex and from complex to simple.

As shown in panels g and h of Figure 5, evolutionary transitions are strongly asymmetric: while complex phenotypes readily regress into simpler ones, the reverse transition proves much harder. Populations starting from simple forms struggle to reach complex targets and often become trapped in suboptimal fitness regions, suggesting that evolving complexity may require substantially longer evolutionary timescales.

3.4. Simulating Adaptive Maternal Effects with Our CA-Based Model

Finally, to demonstrate the heuristic potential of our CA-based model for exploring less well-understood developmental and evolutionary phenomena beyond its alignment with known variational patterns of living systems, we conducted two proof-of-concept sets of simulations.

The first one is an evolutionary experiment concerned with the adaptive role of maternal effects. These refer to epigenetic factors (e.g., hormones, proteins, mRNA gradients) that are maternally provided (i.e., dependent on the maternal phenotype) and influence developmental dynamics, thereby affecting the offspring's phenotype. These effects are widespread in nature: for example, stress-induced hormonal changes in bird eggs can alter hatchling behavior and metabolic profiles [88], and maternally inherited molecular gradients are essential for establishing embryonic axes and enabling gene regulatory networks to function properly in early insect development [28,74,89]. The necessity of maternally provided information is, indeed, a general biological principle, since every organism is, in a non-metaphorical sense, “a detached bit of its parents” [90].

The goal of this experiment was not to provide a detailed or predictive account, but rather to probe the internal consistency of common assumptions about maternal effects in evolutionary theory. This is precisely the kind of insight that toy models like ours are designed to provide, by abstracting biological complexity to highlight key structural and logical constraints (e.g., [30]). In our model, maternal effects were implemented by replacing the usual random mutation of the initial condition **Epi** with a direct inheritance mechanism. Specifically, each offspring's initial conditions were “copied” from the central 4×4 region of its maternal phenotype at generation $t - 1$. In other words, each new individual began its development from a configuration that was a specific subset of its mother's phenotype. All other experimental settings were kept the same as in the standard evolutionary scenario, including the basic mutational algorithm in vector **G** (i.e., as in Figure 5a–d). These simulations, which model unbuffered maternal inheritance, reveal that such maternal effects fail to confer an adaptive advantage. On the contrary, adaptive performance collapses, and fitness fails to improve even when genetic mutations are allowed (Figure 5i,j). This discrepancy with the biological reality and ubiquity of maternally transmitted epigenetic inputs does not reflect a failure of the model. Rather, it highlights a critical feature of such simplified developmental architectures: maternally inherited information, if transmitted too rigidly or without developmental modulation, can become maladaptive. These findings suggest that, for maternal effects to support adaptation, they must either decay quickly across generations or be buffered—i.e., integrated in a way that allows for development to modulate their impact. Revisiting these assumptions may help uncover the conditions under which maternal effects become effectively adaptive (see Section 4).

3.5. Simulating Tumor Growth with Our CA-Based Model

Our second proof-of-concept experiment focuses on tumor evolution and was specifically designed to illustrate (i) how, in certain instances, the model can be translated into an applicable tool for biomedical sciences, and (ii) how our model can generate data that can be *quantitatively* compared with empirical evidence.

In essence, we investigated whether our model could reproduce the spatial dynamics of tumor evolution, which is a critical aspect of cancer research. Such tumor growth can be characterized by multiple features, such as the number of tumor-cell subpopulations that can coexist, the relative size of each subpopulation, or the frequency with which

subpopulations are replaced over developmental time. The first two properties are usually summarized by the clonal diversity index (D), defined as

$$D = 1 / \sum_{i=1}^{MNC} p_i^2 \quad (2)$$

where MNC is the maximum number of tumor-cell subpopulations and p_i represents the size (i.e., number of cells) of each subpopulation relative to the total tumor size. The third property, subpopulation turnover, is measured by the average clonal turnover ($\bar{\Theta}$), defined as the mean of all turnover values $\Theta(t)$ computed at each iteration:

$$\Theta(t) = \sum_{i=1}^{MNC} (p_i(t) + p_i(t - \delta))^2 \quad (3)$$

being δ a time interval of length $0.1 \cdot t_{\max}$. To simulate such tumor evolution using our CA-based model, we introduced a (founder) single-point mutation into one of the living cells of the initial ($t=0$) epigenetic matrix (**Epi**). With a constant mutation rate μ ($10^{-4} < \mu < 10^{-1}$), mutant cells accumulate further mutations. Each new mutation is assigned a unique integer label that defines its clonal identity: all cells sharing the same label are considered part of the same subpopulation. When a mutant cell divides, its daughter inherits the same label, giving rise to clonal lineages. Non-mutated cells, which can be interpreted as the healthy tissue invaded by the tumor, are labeled as zero. D and Θ were recorded for each individual replicate.

Using these minimal assumptions, we first asked whether cancer mutations that affect cell motility alter the expansive dynamics of tumor growth. To address this, we defined two scenarios: (i) NMMS (non-morphogenetic mutations), where mutations do not alter the morphogenetic rules encoded in vector **G**; and (ii) MMS (morphogenetic mutations), where each new mutation randomly modifies one position in **G**, as described in the Section 3.2.

Our simulations show that mutations which alter morphogenetic rules have a similar effect to those that do not in terms of clonal cell diversity and their invasive capacity. (Figure 6a,b). By contrast, mutation rate has a pronounced impact on tumor evolution: while very low rates ($\mu \leq 10^{-4}$) are, as expected, associated with slow expansion and low clonal diversity counts, similar dynamics are also found at very high mutation rates ($\mu \geq 10^{-1}$). Tumor progression seems thus maximized at intermediate mutation rates ($10^{-3} < \mu < 10^{-2}$ in our simulations), likely because they generate spatial dynamics compatible with those of the surrounding tissue, thereby enhancing spatial coupling and invasive potential. Indeed, morphologies resulting from these intermediate mutation rates exhibit a mosaic-like distribution of tumor cells scattered across most parts of the *in silico* “organism” (Figure 6c, central panels). In contrast, excessively high or low mutation rates result in either decohesive, loosely fragmented clusters of fully tumoral cells (Figure 6c, leftmost panel) or, conversely, a few isolated tumor cells embedded within a large mass of healthy tissue (Figure 6c, rightmost panel). These results align with previous findings on the error catastrophe phenomenon in cancer and other biological systems [91–93], underscoring how even minimal models can capture generic yet critical aspects of tumor evolution and thereby enrich the theoretical foundations of biomedical research.

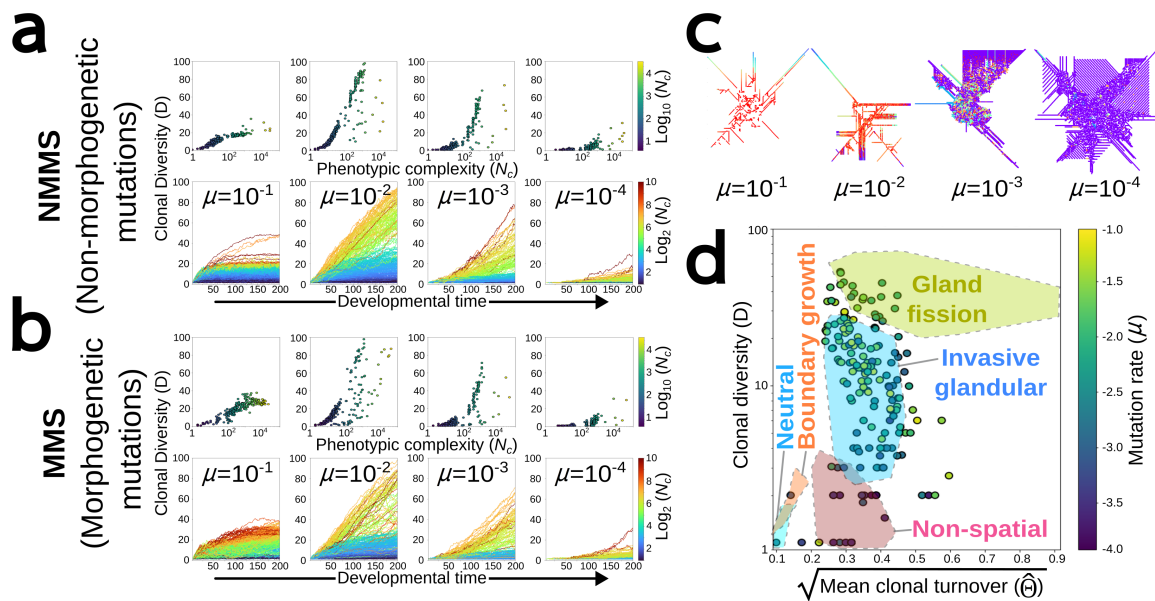


Figure 6. Simulating tumor growth. (a) To simulate tumor evolution with our CA-based model, single-point mutations were introduced in cells under different (constant) mutation rates μ (starting from the initial epigenetic matrix E_{pi}). Initially, these mutations were independent of the vector G encoding the morphogenetic rules (NMMS scenario). The plots show that the number of tumor cell subpopulations (Clonal Diversity index, D) increases non-linearly with phenotypic complexity (upper row) and, less intuitively, follows different growth modes under different mutation rates (lower row). (b) Similar results are obtained under the MMS scenario, where carcinogenetic point mutations affect the rules encoded in the vector G . (c) In the MMS scenario, morphologies resulting from different mutation rates exhibit distinctive patterns in the number and distribution of clonal (tumor) cells (colored dots) within the non-tumoral tissue (purple dots). From left to right: low mutation rates (μ) result in fragmented clusters of fully tumoral cells, intermediate μ result in a mosaic-like distribution of tumor cells, and high μ allows for the growth of a large mass of healthy tissue containing only a few isolated tumor cells. (d) Quantitative comparison of tumor growth metrics with empirical data reveals that, by changing only the mutation rate μ , the MMS setting can reproduce qualitatively different tumor growth dynamics, with the notable exception of the “gland fission” mode (see main text). Each point represents one of the 300 replicates generated by our CA-based model, while translucent convex hulls delineate the point clouds reported in [69]; both axes are plotted on the same scale.

Under these premises, we speculated whether our model could quantitatively mimic the progression of *real* tumors. Recent and influential studies [69,94] have shown that the progression of most tumors can be classified into a few basic modes, depending on the dispersal strategies of tumor cells: non-spatial, gland fission, invasive glandular, and boundary growth. Cancer genomic data and detailed computer simulations have revealed that each of these modes exhibits distinctive patterns in the indices D and Θ , thereby providing a suitable test bench for other models. By comparing these indices between our simulations and those reported in Ref. [69], we found that changes in mutation rates alone can shift the system from one mode of tumor growth to another (Figure 6d), although a simple mapping between μ and growth mode remains elusive. This suggests that, at least in some cases, efficient cancer expansion may not require an orchestrated coordination of cell behaviors or growth rules, but can simply emerge from random alterations applied at sufficiently high frequency. Interestingly, our minimal model is unable to replicate the gland fission mode of growth, in which a single mass of tumor cells splits into several, smaller ones. This limitation may stem from the inability of cells in our

model to migrate or leave intercellular gaps (forbidden by Rule 1), but further investigation is needed to clarify this mechanism and to ensure the broader applicability of our findings.

4. Discussion

Across all levels of biological organization, from gene regulation to tissue morphogenesis and ecological interactions, life displays remarkable complexity. Disentangling this complexity remains a formidable challenge, and computational models have proven to be powerful allies in this endeavor. However, models must face a fundamental trade-off: balancing simplicity and tractability against realism and interpretability. Thus, while developing approaches that can generate rich, biologically meaningful dynamics without incurring prohibitive computational cost is essential for advancing our understanding of evolution and development, achieving this balance remains an elusive goal.

The CA-based model introduced in this paper contributes to the relatively small set of models that occupy this middle ground. It operates using just four simple update rules, each abstracting a fundamental developmental mechanism such as stasis, apoptosis, state change, or directional growth. Despite its abstract nature and minimalist design, and despite the fact that its resulting phenotypes bear little resemblance to known organisms, our results demonstrate that the system exhibits a broad range of emergent behaviors characteristic of developing biological systems. These include self-organization, structured pattern formation, morphogenesis-like dynamics, complex genotype-to-phenotype mappings, and evolvability.

A key feature of our system that contributes to the emergence of non-linearity—and thus to the overall complexity of its generative dynamics—is the phenomenon of *local frustration*. Here, we refer to frustration in a specific, operational sense: it arises when the ideal transformation prescribed by the generative operator \mathcal{R} (see Section 2) is not among the set of physically realizable transitions at time t , denoted $\mathcal{P}(\mathbf{S}^t)$. That is, frustration occurs whenever

$$\mathcal{R}(\mathbf{S}^t, \mathbf{G}) \notin \mathcal{P}(\mathbf{S}^t),$$

reflecting a mismatch between what the generative rule aims to achieve (e.g., directional growth) and what the system can actually perform due to spatial constraints.

In our model, such local frustration primarily results from Rule 3, which governs directional cell growth. This rule “attempts” to modify a neighboring cell rather than the focal cell itself, with success depending on both the internal state of the focal cell and the occupancy of the target site. Since two cells cannot simultaneously occupy the same position in the 2D grid, Rule 3 naturally introduces a form of volume-exclusion principle, which is known to drive the emergence of complex spatial patterns in many physical and biological systems [7,95,96]. Furthermore, these local constraints can propagate and amplify across scales due to the iterative nature of our CA-based model, potentially giving rise to the emergent properties and higher-order structures not explicitly encoded in the rule set.

However, in contrast to many standard CPMs and some CA-based models, where these exclusion effects are typically enforced via non-local energy minimization terms (e.g., area/perimeter constraints), in our case, this spatial conflict emerges directly from the local update logic. This spatiotemporal dependency makes our CA-based model only weakly compatible with standard CA formalisms and transition matrices [29,37,66], yet more aligned with recent minimal asynchronous approaches implementing similar mechanisms [29,55,97,98]. From this perspective, while our CA-based model does not constitute a genuinely new class within the vast catalog of CA models [29,52], our specific instantiation, characterized by inherent cell directionality and internal cyclic states, remains among the algorithmically simplest. This simplicity alleviates some of the complications of

non-locality and non-equilibrium that pervade more complex models [63], and appears particularly well suited, to study generic and abstract genotype–phenotype relationships.

From a probabilistic perspective, this emergent volume-exclusion principle likely underlies the complexity–frequency anticorrelation observed in our model. This is because, although the probability of the system decreasing in size, $p(N_c(t+1) < N_c(t)) = p(\text{rule 1, apoptosis}) = 1/4$, or of remaining the same size, $p(N_c(t+1) = N_c(t)) = p(\text{rule 0}) + p(\text{rule 2}) = 1/2$, is fixed, the probability of increasing the system’s size changes dynamically and decreases as the average cell density increases, since most surrounding sites are likely to be occupied. Therefore, although the nominal probability of growth is constant, $p(\text{rule 3}) = 1/4$, the probability of actual growth is always smaller. It ranges from $(1/4) \times (7/9) \approx 0.194$ when cells have, on average, one neighbor (the case of zero neighbors is excluded by rule 1), down to zero when cells have, on average, nine neighbors, leaving no vacant sites for expansion. In practice, growth may still occur at the system’s boundary, even in the case of a nearly solid and densely packed square. However, in this case, the perimeter-to-area ratio (and thus the probability of further growth) decreases as $4/\sqrt{N_c}$, becoming vanishingly small as the number of cells increases. This density dependence introduces a negative feedback, or ratchet-like mechanism, whereby larger phenotypes are increasingly unlikely to continue growing, strongly hindering further increases in complexity and skewing the complexity distributions toward the simplest cases.

In an evolutionary context, this form of structured variation gives rise to developmental biases and non-zero evolvability, contributing to the emergence of asymmetric phenotypic transitions, where it is generally easier to evolve from complex to simple forms than the reverse [12,86,87]. This pattern is clearly observed in our targeted simulations involving directional transitions between phenotypes of differing complexity (Figure 5g,h). As in biological systems, the asymmetry arises from the unequal likelihood and distribution of simple and complex phenotypes within the search space. Because complex forms are much rarer and more sparsely distributed, most mutants surrounding a given phenotype will, statistically, correspond to simpler configurations. As a result of this anisotropy in the local mutational neighborhood, accumulating and maintaining mutations that increase complexity is both more difficult and more time-consuming than transitions toward simpler phenotypes, which tend to follow paths of least resistance.

By reproducing these key variational properties observed in biological systems from minimal assumptions, our CA-based model provides a coherent framework for investigating broader evolutionary phenomena, particularly those involving an interplay between selective forces and the constraints imposed by the system’s structural and spatial features. This explanatory capacity is exemplified in our final experiments, which explore, respectively, the evolutionary dynamics of adaptive maternal effects and tumor growth. The first experiment reveals that when maternal influences are transmitted in every generation and exert a dominant role in phenotype determination, adaptive evolution is severely compromised. This observation suggests that for maternal effects to be truly adaptive, they cannot simultaneously be both long-lasting (i.e., span multiple generations) and strongly deterministic. In other words, either maternal inputs must decay rapidly over evolutionary time, or developmental processes must buffer their influence on phenotypes. This buffering would help to ensure that development remains relatively insensitive to variation in the maternally provided epigenetic inputs. Notably, this insight aligns with empirical observations in natural systems, where maternal effects typically have limited phenotypic consequences [99] and rarely persist across generations [100], often reflecting transient environmental conditions.

In turn, our second case-study experiment suggests that pure mutational noise can drive transitions between qualitatively different tumor growth dynamics and that invasive

potential is maximized when the growth rates of tumors and the surrounding tissues are concordant. Taken together, these two experiments illustrate how our CA-based model, through its algorithmic simplicity and ease of implementation, provides a promising heuristic tool for addressing theoretical questions at the interface between generative rules and evolutionary processes, while also showcasing its flexibility to incorporate additional features (which might easily include others such as extra internal states and non-gradual transitions between them, new cell behaviors, chemical signaling, or alternative neighborhood topologies). In both cases, the model yields simple and coherent insights grounded in structural constraints and logical necessity rather than adaptive reasoning—an approach that may, in turn, inform other explanatory levels in evolutionary developmental biology and biomedical research.

To conclude, although our CA-based model is far from universal, it seems to capture certain abstract yet fundamental principles underlying living, developing, and evolving biological systems. The appearance of life-like variational properties in a system as simple as ours implies that certain features of living systems may be governed not solely by physicochemical principles, but also by deeper, more universal organizational principles grounded in generative logic. Identifying such principles and clarifying their contribution to the complexity of living systems could represent a promising direction for future research, and our CA-based model may serve as a useful tool in that endeavor.

Author Contributions: Conceptualization, M.B.-U.; methodology, M.B.-U. and R.L.; software, J.d.J.G.; validation, M.B.-U., J.d.J.G. and R.L.; formal analysis, M.B.-U., J.d.J.G. and R.L.; investigation, M.B.-U. and J.d.J.G.; resources, M.B.-U., J.d.J.G. and R.L.; data curation, J.d.J.G.; writing—original draft preparation, M.B.-U. and R.L.; writing—review and editing, M.B.-U., J.d.J.G. and R.L.; visualization, M.B.-U. and J.d.J.G.; supervision, M.B.-U. and R.L.; project administration, M.B.-U. All authors have read and agreed to the published version of the manuscript.

Funding: This research received no external funding.

Data Availability Statement: No new empirical data were generated or analyzed in this study. All results derive from simulations that can be fully reproduced by running the computational model, written in Fortran, which is openly available at <https://github.com/rlatorre-uam/ca-developmental-model.git> (accessed on 1 October 2025).

Acknowledgments: The authors thank Irene Hernando-Herraez, Jesús Ortega, and Roland Zimm for their helpful feedback and proofreading. They are also grateful to the Evolutionary Biology group at Lund University, where the initial ideas for this study were conceived. M.B.U. would like to express special thanks to Cristina Marzo, whose support was essential for the completion of this work, and lovingly dedicates it to Roldán, recently born, with the hope that curiosity and wonder always accompany him.

Conflicts of Interest: The authors declare no conflicts of interest.

Abbreviations

The following abbreviations are used in this manuscript:

CA	Cellular Automaton
D	Clonal Diversity (for Tumor growth simulations)
Epi	Epigenetic Matrix
G	Genetic Vector
GHD	Genetic Hamming Distance
GPM	Genotype-to-Phenotype Map
GRN	Gene Regulatory Network
H	Shannon Entropy
HD	Hausdorff Dimension (i.e., “Fractality”)

MMS	Morphogenetic Mutations Scenario
NMMS	Non-Morphogenetic Mutations Scenario
PED	Phenotypic Euclidean Distance
PHD	Phenotypic Hamming Distance
T	Target Phenotype (for Evolutionary Simulations)
W	Fitness (for Evolutionary Simulations)

References

1. Kauffman, S.A. The origins of order: Self-organization and selection in evolution. In *Spin Glasses and Biology*; World Scientific: Singapore, 1992; pp. 61–100.
2. Prigogine, I. *Order Out of Chaos: Man's New Dialogue with Nature*; Verso: London, UK, 2017.
3. Belousov, L. *The Dynamic Architecture of a Developing Organism*; Springer: Berlin/Heidelberg, Germany, 1998.
4. Thompson, D.W. *On Growth and Form*, 1st ed.; Cambridge University Press: Cambridge, UK, 1917.
5. Goodwin, B. *How the Leopard Changed Its Spots: The Evolution of Complexity*; Princeton University Press: Princeton, NJ, USA, 2001.
6. Salazar-Ciudad, I.; Jernvall, J.; Newman, S.A. Mechanisms of pattern formation in development and evolution. *Development* **2003**, *130*, 2027–2037. [[CrossRef](#)] [[PubMed](#)]
7. Forgacs, G.; Newman, S.A. *Biological Physics of the Developing Embryo*; Cambridge University Press: Cambridge, UK, 2005.
8. Newman, S.A.; Bhat, R. Dynamical patterning modules: A “pattern language” for development and evolution of multicellular form. *Int. J. Dev. Biol.* **2009**, *53*, 693–705. [[CrossRef](#)]
9. Alberch, P. From genes to phenotype: Dynamical systems and evolvability. *Genetica* **1991**, *84*, 5–11. [[CrossRef](#)]
10. Brun-Usan, M.; Zimm, R.; Uller, T. Beyond genotype-phenotype maps: Toward a phenotype-centered perspective on evolution. *BioEssays* **2022**, *44*, 2100225. [[CrossRef](#)] [[PubMed](#)]
11. Salazar-Ciudad, I.; Marín-Riera, M. Adaptive dynamics under development-based genotype–phenotype maps. *Nature* **2013**, *497*, 361–364. [[CrossRef](#)]
12. Harjunmaa, E.; Kallonen, A.; Voutilainen, M.; Hämäläinen, K.; Mikkola, M.L.; Jernvall, J. On the difficulty of increasing dental complexity. *Nature* **2012**, *483*, 324–327. [[CrossRef](#)]
13. Uller, T.; Moczek, A.P.; Watson, R.A.; Brakefield, P.M.; Laland, K.N. Developmental Bias and Evolution: A Regulatory Network Perspective. *Genetics* **2018**, *209*, 949–966. [[CrossRef](#)]
14. Gavrilits, S. Evolution and speciation on holey adaptive landscapes. *Trends Ecol. Evol.* **1997**, *12*, 307–312. [[CrossRef](#)]
15. Gould, S.J. *The Structure of Evolutionary Theory*; Harvard University Press: Cambridge, MA, USA; London, UK, 2002.
16. Galis, F.; Metz, J.A.; van Alphen, J.J. Development and Evolutionary Constraints in Animals. *Annu. Rev. Ecol. Evol. Syst.* **2018**, *49*, 499–522. [[CrossRef](#)]
17. Raup, D.M. The geometry of coiling in gastropods. *Proc. Natl. Acad. Sci. USA* **1961**, *47*, 602–609. [[CrossRef](#)] [[PubMed](#)]
18. Maynard Smith, J.; Burian, R.M.; Kauffman, S.; Alberch, P.; Campbell, J.; Goodwin, B.; Lande, R.; Raup, D.; Wolpert, L. Developmental Constraints and Evolution: A Perspective from the Mountain Lake Conference on Development and Evolution. *Q. Rev. Biol.* **1985**, *60*, 265–287. [[CrossRef](#)]
19. Roff, D. The evolution of the G matrix: Selection or drift? *Heredity* **2000**, *84*, 135–142. [[CrossRef](#)]
20. Rice, S.H. Theoretical Approaches to the Evolution of Development and Genetic Architecture. *Ann. N. Y. Acad. Sci.* **2008**, *1133*, 67–86. [[CrossRef](#)]
21. McGhee, G.R. *The Geometry of Evolution: Adaptive Landscapes and Theoretical Morphospaces*; Cambridge University Press: Cambridge, UK, 2006.
22. Honda, H.; Tanemura, M.; Nagai, T. A three-dimensional vertex dynamics cell model of space-filling polyhedra simulating cell behavior in a cell aggregate. *J. Theor. Biol.* **2004**, *226*, 439–453. [[CrossRef](#)] [[PubMed](#)]
23. Sandersius, S.A.; Newman, T.J. Modeling cell rheology with the Subcellular Element Model. *Phys. Biol.* **2008**, *5*, 015002. [[CrossRef](#)] [[PubMed](#)]
24. Okuda, S.; Inoue, Y.; Adachi, T. Three-dimensional vertex model for simulating multicellular morphogenesis. *Biophys. Physicobiol.* **2015**, *12*, 13–20. [[CrossRef](#)] [[PubMed](#)]
25. Marín-Riera, M.; Brun-Usan, M.; Zimm, R.; Välikangas, T.; Salazar-Ciudad, I. Computational modeling of development by epithelia, mesenchyme and their interactions: A unified model. *Bioinformatics* **2016**, *32*, 219–225. [[CrossRef](#)]
26. Nissen, S.B.; Rønild, S.; Trusina, A.; Sneppen, K. Theoretical tool bridging cell polarities with development of robust morphologies. *eLife* **2018**, *7*, e38407. [[CrossRef](#)]
27. Hogeweg, P. Evolving Mechanisms of Morphogenesis: On the Interplay between Differential Adhesion and Cell Differentiation. *J. Theor. Biol.* **2000**, *203*, 317–333. [[CrossRef](#)]

28. Salazar-Ciudad, I.; Solé, R.V.; Newman, S.A. Phenotypic and dynamical transitions in model genetic networks II. Application to the evolution of segmentation mechanisms. *Evol. Dev.* **2001**, *3*, 95–103. [\[CrossRef\]](#)
29. Osborne, J.M.; Fletcher, A.G.; Pitt-Francis, J.M.; Maini, P.K.; Gavaghan, D.J. Comparing individual-based approaches to modelling the self-organization of multicellular tissues. *PLoS Comput. Biol.* **2017**, *13*, e1005387. [\[CrossRef\]](#)
30. Levins, R. The Strategy of Model Building in Population Biology. *Am. Sci.* **1966**, *54*, 421–431.
31. Arnold, S.J.; Bürger, R.; Hohenlohe, P.A.; Ajie, B.C.; Jones, A.G. Understanding the evolution and stability of the G-matrix. *Evolution* **2008**, *62*, 2451–2461. [\[CrossRef\]](#)
32. Hansen, T.F.; Wagner, G.P. Modeling Genetic Architecture: A Multilinear Theory of Gene Interaction. *Theor. Popul. Biol.* **2001**, *59*, 61–86. [\[CrossRef\]](#) [\[PubMed\]](#)
33. Draghi, J.; Wagner, G.P. Evolution of Evolvability in a developmental model. *Evolution* **2008**, *62*, 301–315. [\[CrossRef\]](#) [\[PubMed\]](#)
34. Pavlicev, M.; Cheverud, J.M.; Wagner, G.P. Evolution of adaptive phenotypic variation patterns by direct selection for evolvability. *Proc. R. Soc. B Biol. Sci.* **2011**, *278*, 1903–1912. [\[CrossRef\]](#)
35. Hallgrímsson, B.; Jamniczky, H.A.; Young, N.M.; Rolian, C.; Schmidt-Ott, U.; Marcucio, R.S. The generation of variation and the developmental basis for evolutionary novelty. *J. Exp. Zool. Part B Mol. Dev. Evol.* **2012**, *318*, 501–517. [\[CrossRef\]](#)
36. Von Neumann, J. Theory of self-reproducing automata. *IEEE Trans. Neural Netw.* **1966**, *5*, 3–14.
37. Toffoli, T.; Margolus, N. *Cellular Automata Machines: A New Environment for Modeling*; MIT Press: Cambridge, MA, USA, 1987.
38. Ilachinski, A. *Cellular Automata: A Discrete Universe*; World Scientific Publishing Company: Singapore, 2001.
39. Izhikevich, E.M.; Conway, J.H.; Seth, A. Game of life. *Scholarpedia* **2015**, *10*, 1816. [\[CrossRef\]](#)
40. Gardner, M. Mathematical Games. *Sci. Am.* **1970**, *223*, 120–123. [\[CrossRef\]](#)
41. Weisstein, E.W. Game of Life. MathWorld—A Wolfram Web Resource. 2002. Available online: <https://mathworld.wolfram.com/GameofLife.html> (accessed on 1 October 2025).
42. Saadat, M. Cellular Automata in the Triangular Grid. Master's Thesis, Eastern Mediterranean University (EMU)-Doğu Akdeniz Üniversitesi (DAÜ), Famagusta, Cyprus, 2016.
43. Woods, D.; Neary, T. The complexity of small universal Turing machines: A survey. *Theor. Comput. Sci.* **2009**, *410*, 443–450. [\[CrossRef\]](#)
44. Chan, B.W.C. Lenia and Expanded Universe. In Proceedings of the ALIFE 2020: The 2020 Conference on Artificial Life, Online, 13–18 July 2020; Artificial Life Conference Proceedings; MIT Press: Cambridge, MA, USA, 2020; pp. 221–229. [\[CrossRef\]](#)
45. Caballero, L.; Germinal, C.; Sergio, H. Game of Life: Simple interactions ecology. In *Frontiers in Ecology, Evolution and Complexity*; TS0012EN; Benítez, M., Miramontes, O., Valiente-Banuet, A., Eds.; CopIt ArXives: Mexico City, Mexico, 2014.
46. Caballero, L.; Hodge, B.; Hernandez, S. Conway's "Game of Life" and the Epigenetic Principle. *Front. Cell. Infect. Microbiol.* **2016**, *6*, 57. [\[CrossRef\]](#)
47. Waddington, C.H. *New Patterns in Genetics and Development*; Columbia University Press: New York, NY, USA, 1962.
48. Jablonka, E.; Lamb, M.J. The inheritance of acquired epigenetic variations. *Int. J. Epidemiol.* **2015**, *44*, 1094–1103. [\[CrossRef\]](#)
49. Hagolani, P.F.; Zimm, R.; Marin-Riera, M.; Salazar-Ciudad, I. Cell signaling stabilizes morphogenesis against noise. *Development* **2019**, *146*, dev179309. [\[CrossRef\]](#)
50. Petak, C.; Frati, L.; Vroomans, R.M.; Pespeni, M.H.; Cheney, N. The variability of evolvability: Properties of dynamic fitness landscapes determine how phenotypic variability evolves. *bioRxiv* **2025**. [\[CrossRef\]](#)
51. Graner, F.; Glazier, J.A. Simulation of biological cell sorting using a two-dimensional extended Potts model. *Phys. Rev. Lett.* **1992**, *69*, 2013–2016. [\[CrossRef\]](#) [\[PubMed\]](#)
52. Swat, M.H.; Thomas, G.L.; Belmonte, J.M.; Shirinifard, A.; Hmeljak, D.; Glazier, J.A. Multi-scale modeling of tissues using CompuCell3D. *Methods Cell Biol.* **2012**, *110*, 325–366. [\[CrossRef\]](#)
53. Canty, L.; Zarour, E.; Kashkooli, L.; François, P.; Fagotto, F. Sorting at embryonic boundaries requires high heterotypic interfacial tension. *Nat. Commun.* **2017**, *8*, 157. [\[CrossRef\]](#) [\[PubMed\]](#)
54. Franke, F.; Aland, S.; Böhme, H.J.; Voss-Böhme, A.; Lange, S. Is cell segregation like oil and water: Asymptotic versus transitory regime. *PLoS Comput. Biol.* **2022**, *18*, e1010460. [\[CrossRef\]](#)
55. Lange, S.; Schmied, J.; Willam, P.; Voss-Böhme, A. Minimal cellular automaton model with heterogeneous cell sizes predicts epithelial colony growth. *J. Theor. Biol.* **2024**, *592*, 111882. [\[CrossRef\]](#) [\[PubMed\]](#)
56. Kuang, X.; Guan, G.; Tang, C.; Zhang, L. MorphoSim: An efficient and scalable phase-field framework for accurately simulating multicellular morphologies. *NPJ Syst. Biol. Appl.* **2023**, *9*, 6. [\[CrossRef\]](#) [\[PubMed\]](#)
57. Starrau, J.; de Back, W.; Brusch, L.; Deutsch, A. Morpheus: A user-friendly modeling environment for multiscale and multicellular systems biology. *Bioinformatics* **2014**, *30*, 1331–1332. [\[CrossRef\]](#)
58. Mirams, G.R.; Arthurs, C.J.; Bernabeu, M.O.; Bordas, R.; Cooper, J.; Corrias, A.; Davit, Y.; Dunn, S.J.; Fletcher, A.G.; Harvey, D.G.; et al. Chaste: An open source C++ library for computational physiology and biology. *PLoS Comput. Biol.* **2013**, *9*, e1002970. [\[CrossRef\]](#)

59. Izaguirre, J.A.; Chaturvedi, R.; Huang, C.; Cickovski, T.; Coffland, J.; Thomas, G.; Forgacs, G.; Alber, M.; Hentschel, G.; Newman, S.A.; et al. CompuCell, a multi-model framework for simulation of morphogenesis. *Bioinformatics* **2004**, *20*, 1129–1137. [\[CrossRef\]](#)
60. Libby, A.R.; Briers, D.; Haghighi, I.; Joy, D.A.; Conklin, B.R.; Belta, C.; McDevitt, T.C. Automated Design of Pluripotent Stem Cell Self-Organization. *Cell Syst.* **2019**, *9*, 483–495.e10. [\[CrossRef\]](#)
61. Nelemans, B.K.; Schmitz, M.; Tahir, H.; Merks, R.M.; Smit, T.H. Somite Division and New Boundary Formation by Mechanical Strain. *iScience* **2020**, *23*, 100976. [\[CrossRef\]](#) [\[PubMed\]](#)
62. Chopard, B.; Droz, M. *Cellular Automata Modeling of Physical Systems*; Cambridge University Press: Cambridge, UK, 1998. [\[CrossRef\]](#)
63. Voss-Böhme, A. Multi-scale modeling in morphogenesis: A critical analysis of the cellular potts model. *PLoS ONE* **2012**, *7*, e42852. [\[CrossRef\]](#)
64. Killeen, A.; Partridge, B.; Bertrand, T.; Lee, C.F. Modeling growing confluent tissues using a lattice Boltzmann method: Interface stability and fluctuations. *Phys. Rev. Res.* **2023**, *5*, 043096. [\[CrossRef\]](#)
65. Alert, R.; Treppe, X. Physical models of collective cell migration. *Annu. Rev. Condens. Matter Phys.* **2020**, *11*, 77–101. [\[CrossRef\]](#)
66. Wolfram, S. Statistical mechanics of cellular automata. *Rev. Mod. Phys.* **1983**, *55*, 601–644. [\[CrossRef\]](#)
67. Crombach, A.; Hogeweg, P. Evolution of evolvability in gene regulatory networks. *PLoS Comput. Biol.* **2008**, *4*, e1000112. [\[CrossRef\]](#)
68. Hernández-Hernández, V.; Niklas, K.J.; Newman, S.A.; Benítez, M. Dynamical patterning modules in plant development and evolution. *Int. J. Dev. Biol.* **2012**, *56*, 661–674. [\[CrossRef\]](#)
69. Noble, R.; Burri, D.; Kather, J.N.; Beerenwinkel, N. Spatial structure governs the mode of tumour evolution. *Nat. Ecol. Evol.* **2022**, *6*, 207–217. [\[CrossRef\]](#) [\[PubMed\]](#)
70. Chopard, B.; Ouared, R.; Deutsch, A.; Hatzikirou, H.; Wolf-Gladrow, D. Lattice-gas cellular automaton models for biology: From fluids to cells. *Acta Biotheor.* **2010**, *58*, 329–340. [\[CrossRef\]](#) [\[PubMed\]](#)
71. Ofria, C.; Wilke, C.O. Avida: A Software Platform for Research in Computational Evolutionary Biology. *Artif. Life* **2004**, *10*, 191–229. [\[CrossRef\]](#) [\[PubMed\]](#)
72. Fisher, R.A. *The Genetical Theory of Natural Selection*; Clarendon Press: Oxford, UK, 1930.
73. Kimura, M. On the Probability of Fixation of Mutant Genes in a Population. *Genetics* **1962**, *47*, 713–719. [\[CrossRef\]](#)
74. Gilbert, S.F.; Raunio, A.M. *Embryology: Constructing the Organism*; Sinauer Associates: Sunderland, MA, USA, 1997.
75. Fontana, W.; Schuster, P. Shaping Space: The Possible and the Attainable in RNA Genotype–phenotype Mapping. *J. Theor. Biol.* **1998**, *194*, 491–515. [\[CrossRef\]](#)
76. Levin, M.; Anavy, L.; Cole, A.G.; Winter, E.; Mostov, N.; Khair, S.; Senderovich, D.; Kovalev, E.; Silver, D.H.; Feder, M.; et al. The mid-developmental transition and the evolution of animal body plans. *Nature* **2016**, *531*, 637–641. [\[CrossRef\]](#)
77. Jiménez, A.; Cotterell, J.; Munteanu, A.; Sharpe, J. Dynamics of gene circuits shapes evolvability. *Proc. Natl. Acad. Sci. USA* **2015**, *112*, 2103–2108. [\[CrossRef\]](#)
78. Chaitin, G.J. Information-Theoretic Limitations of Formal Systems. *J. ACM* **1974**, *21*, 403–424. [\[CrossRef\]](#)
79. Hagolani, P.F.; Zimm, R.; Vroomans, R.; Salazar-Ciudad, I. On the evolution and development of morphological complexity: A view from gene regulatory networks. *PLoS Comput. Biol.* **2021**, *17*, e1008570. [\[CrossRef\]](#)
80. DiFrisco, J.; Jaeger, J. Beyond networks: Mechanism and process in evo-devo. *Biol. Philos.* **2019**, *34*, 54. [\[CrossRef\]](#)
81. Katatbeh, Q.D.; Martínez-Aroza, J.; Gómez-Lopera, J.F.; Blanco-Navarro, D. An Optimal Segmentation Method Using Jensen–Shannon Divergence via a Multi-Size Sliding Window Technique. *Entropy* **2015**, *17*, 7996–8006. [\[CrossRef\]](#)
82. Falconer, K. *Fractal Geometry: Mathematical Foundations and Applications*, 2nd ed.; Wiley: Hoboken, NJ, USA, 2003.
83. Mandelbrot, B.B. *The Fractal Geometry of Nature*; W. H. Freeman and Company: New York, NY, USA, 1982.
84. Furusawa, C.; Kaneko, K. Formation of dominant mode by evolution in biological systems. *Phys. Rev. E* **2018**, *97*, 042410. [\[CrossRef\]](#)
85. Wilke, C.O. Adaptive Evolution on Neutral Networks. *Bull. Math. Biol.* **2001**, *63*, 715–730. [\[CrossRef\]](#) [\[PubMed\]](#)
86. Brun-Usan, M.; Thies, C.; Watson, R.A. How to fit in: The learning principles of cell differentiation. *PLoS Comput. Biol.* **2020**, *16*, e1006811. [\[CrossRef\]](#) [\[PubMed\]](#)
87. Zimm, R.; Berio, F.; Debiais-Thibaud, M.; Goudemand, N. A shark-inspired general model of tooth morphogenesis unveils developmental asymmetries in phenotype transitions. *Proc. Natl. Acad. Sci. USA* **2023**, *120*, e2216959120. [\[CrossRef\]](#) [\[PubMed\]](#)
88. Uller, T. Developmental plasticity and the evolution of parental effects. *Trends Ecol. Evol.* **2008**, *23*, 432–438. [\[CrossRef\]](#) [\[PubMed\]](#)
89. Driever, W.; Nüsslein-Volhard, C. A gradient of bicoid protein in *Drosophila* embryos. *Cell* **1988**, *54*, 83–93. [\[CrossRef\]](#)
90. Wells, H.G.; Huxley, J.; Wells, G.P. *The Science of Life: A Summary of Contemporary Knowledge About Life and Its Possibilities*; Cassell and Company: London, UK, 1929; Volume I.
91. Eigen, M. Selforganization of Matter and the Evolution of Biological Macromolecules. *Naturwissenschaften* **1971**, *58*, 465–523. [\[CrossRef\]](#)
92. Solé, R.V.; Deisboeck, T.S. An error catastrophe in cancer? *J. Theor. Biol.* **2004**, *228*, 47–54. [\[CrossRef\]](#) [\[PubMed\]](#)

93. Loeb, L.A. Human cancers express mutator phenotypes: Origin, consequences and targeting. *Nat. Rev. Cancer* **2011**, *11*, 450–457. [[CrossRef](#)]
94. Maley, C.C.; Aktipis, A.; Graham, T.A.; Sottoriva, A.; Boddy, A.M.; Janiszewska, M.; Silva, A.F.; Gerlinger, M.; Yuan, Y.; Pienta, K.J.; et al. Classifying the evolutionary and ecological features of neoplasms. *Nat. Rev. Cancer* **2017**, *17*, 605–619. [[CrossRef](#)]
95. Kajita, A.; Yamamura, M.; Kohara, Y. Computer simulation of the cellular arrangement using physical model in early cleavage of the nematode *Caenorhabditis elegans*. *Bioinformatics* **2003**, *19*, 704–716. [[CrossRef](#)]
96. Zhang, Q.; Li, J.; Nijjer, J.; Lu, H.; Kothari, M.; Alert, R.; Cohen, T.; Yan, J. Morphogenesis and cell ordering in confined bacterial biofilms. *Proc. Natl. Acad. Sci. USA* **2021**, *118*, e2107107118. [[CrossRef](#)] [[PubMed](#)]
97. Hardy, J.; Pomeau, Y.; de Pazzis, O. Time evolution of a two-dimensional classical lattice system. *Phys. Rev. Lett.* **1973**, *31*, 276–279. [[CrossRef](#)]
98. Deutsch, A.; Dormann, S. *Cellular Automaton Modeling of Biological Pattern Formation*; Birkhäuser: Boston, MA, USA, 2005.
99. He, F.; Wen, Y.; Deng, J.; Lin, X.; Lu, L.J.; Jiao, R.; Ma, J. Probing intrinsic properties of a robust morphogen gradient in *Drosophila*. *Dev. Cell* **2008**, *15*, 558–567. [[CrossRef](#)] [[PubMed](#)]
100. Badyaev, A.V.; Uller, T. Parental effects in ecology and evolution: Mechanisms, processes and implications. *Philos. Trans. R. Soc. B Biol. Sci.* **2009**, *364*, 1169–1177. [[CrossRef](#)]

Disclaimer/Publisher’s Note: The statements, opinions and data contained in all publications are solely those of the individual author(s) and contributor(s) and not of MDPI and/or the editor(s). MDPI and/or the editor(s) disclaim responsibility for any injury to people or property resulting from any ideas, methods, instructions or products referred to in the content.